

Homogeneous Catalysis | Hot Paper |

Design Platform for Sustainable Catalysis with Radicals:
Electrochemical Activation of Cp_2TiCl_2 for Catalysis UnveiledTobias Hilche,^[a] Philip H. Reinsberg,^[b] Sven Klare,^[a] Theresa Liedtke,^[a] Luise Schäfer,^[a] and Andreas Gansäuer^{*[a]}

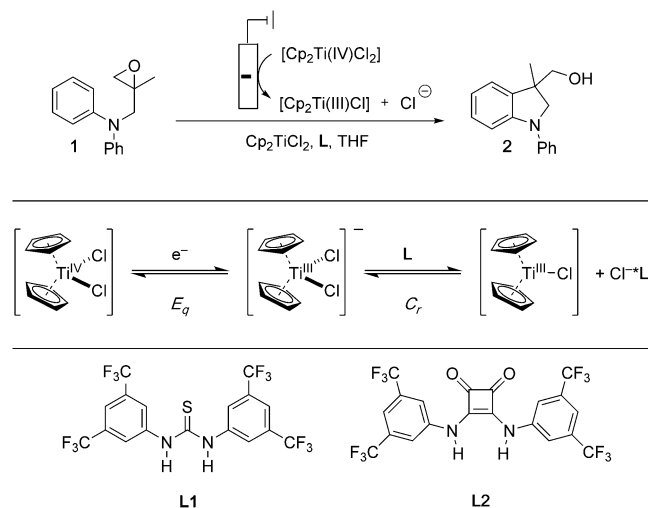
Abstract: The combination of synthesis, rotating ring-disk electrode (RRDE) and cyclic voltammetry (CV) measurements, and computational investigations with the aid of DFT methods shows how a thiourea, a squaramide, and a bisulfonamide as additives affect the E_qC_r equilibrium of Cp_2TiCl_2 . We have, for the first time, provided quantitative data for the E_qC_r equilibrium and have determined the stoichiometry of adduct formation of $[\text{Cp}_2\text{Ti(III)Cl}_2]^-$, $[\text{Cp}_2\text{Ti(III)Cl}]$ and

$[\text{Cp}_2\text{Ti(IV)Cl}_2]$ and the additives. By studying the structures of the complexes formed by DFT methods, we have established the Gibbs energies and enthalpies of complex formation as well as the adduct structures. The results not only demonstrate the correctness of our use of the E_qC_r equilibrium as predictor for sustainable catalysis. They are also a design platform for the development of novel additives in particular for enantioselective catalysis.

Introduction

Catalysis has shaped our modern society, providing functional molecules, materials, or processes both in the lab and on industrial scale. Substituting stoichiometric reactions by catalytic alternatives offers a conceptionally straightforward approach to a more sustainable, green chemistry.^[1] However, as simple this idea may appear in principle, identifying the optimal catalytic conditions usually demands laborious experimental reaction screening through expensive use of workforce, material and laboratory time. To reinforce the sustainability claim of catalysis, we propose to identify mechanistic key aspects or so-called “predictors” before setting up any reaction, avoiding both the *tour de force* and even the designed experimental investigation of the overall catalytic reaction. With these mechanistic key features at hand, we can then predict the optimal catalytic reaction condition based on scientific arguments rather than our usual into the blue approach, so that ideally only a few experimental combinations need to be verified. These “predictors” require either the knowledge of the overall mechanism or at least an understanding of the essentials of

the catalytic cycle. We chose to illustrate our “predictor” concept with the optimization of electrochemical epoxide arylation. It is only after we exploit widely used and readily available cyclic voltammetry (CV) and DFT techniques to identify the “predictors” of this reaction that we enter the synthesis lab to try our smart guess. For catalysis in single electron steps^[2] or metalloradical catalysis,^[3] cyclic voltammetry (CV) is particularly an ideal screening technique because the metals shuttle between neighboring oxidation states. Here, we demonstrate that the E_qC_r equilibrium^[4] is a predictor for the performance of the electrochemical, titanocene catalyzed radical epoxide arylation, providing understanding of the catalyst formation by bulk electrolysis of precatalyst Cp_2TiCl_2 in THF (Scheme 1).^[5] For



Scheme 1. Radical arylation after electrochemical activation (top) and E_qC_r equilibrium of Cp_2TiCl_2 (middle). L denotes anion receptors allowing a shift of the E_qC_r equilibrium by reversible cleaving of Cl^- through hydrogen bonding.

[a] T. Hilche, Dr. S. Klare, Dr. T. Liedtke, L. Schäfer, Prof. Dr. A. Gansäuer
Kekulé-Institut für Organische Chemie und Biochemie
Universität Bonn, Gerhard-Domagk-Straße 1, 53121 Bonn (Germany)
E-mail: andreas.gansaer@uni-bonn.de

[b] Dr. P. H. Reinsberg
Institut für Physikalische und Theoretische Chemie
Universität Bonn, Römerstraße 164, 53117 Bonn (Germany)

Supporting information and the ORCID identification number(s) for the author(s) of this article can be found under:
<https://doi.org/10.1002/chem.202004519>.

© 2020 The Authors. Chemistry - A European Journal published by Wiley-VCH GmbH. This is an open access article under the terms of the Creative Commons Attribution License, which permits use, distribution and reproduction in any medium, provided the original work is properly cited.

a successful electrochemical reduction of $[\text{Cp}_2\text{Ti(IV)Cl}_2]$ the initial product of electron transfer $[\text{Cp}_2\text{Ti(III)Cl}_2]^-$ at the electrode must be transformed into arylation catalyst $[\text{Cp}_2\text{Ti(III)Cl}]$, that is—in contrast to $[\text{Cp}_2\text{Ti(III)Cl}_2]^-$ —easily soluble in THF and can diffuse from the electrode. Increasing the concentration of $[\text{Cp}_2\text{Ti(III)Cl}]$ by halide abstraction from $[\text{Cp}_2\text{Ti(III)Cl}_2]^-$ will therefore facilitate bulk electrolysis of $[\text{Cp}_2\text{Ti(IV)Cl}_2]$. While $[\text{Cp}_2\text{Ti(III)Cl}]$ constitutes the active catalyst for epoxide arylation, $[\text{Cp}_2\text{Ti(III)Cl}_2]^-$ provides a catalytic resting state, that prevents undesired catalyst decomposition.^[6c]

Adjusting the relative amounts of both species in a reversible way thus allows a fine-tuning of the performance of the catalytic system. It turned out that the E_{qC_r} equilibrium and therefore bulk electrolysis of $[\text{Cp}_2\text{Ti(IV)Cl}_2]$ in THF can be controlled by the addition of supramolecular additives, that bind halides through hydrogen bonding.^[7] We show then that the control of the E_{qC_r} equilibrium directly translates into the synthetic performance of the catalytic radical arylation^[6] in THF.

Here, we demonstrate that our qualitative analysis of the cyclic voltammograms (CVs) of the E_{qC_r} equilibrium as predictor for the radical arylation is applicable to bisulfonamides as another class of supramolecular additives. Moreover, it is in accord with quantitative measurements at the rotating ring-disk electrode (RRDE).^[8] The combination of the experimental results with the DFT studies of the intermediates of the E_{qC_r} equilibrium delivers a complete mechanistic analysis of our predictor. Our study not only leads to a better understanding of the systems already investigated. It also delivers a design platform for the use of supramolecular halide binders in enantioselective catalysis and for their use with complexes of metals other than titanium.

Results and Discussion

Cyclic voltammetry and radical arylation

A critical aspect for efficient screening is a fast and cost-efficient technique for a conclusive description of the investigated system. In our case, CV^[9] is an ideal tool because the E_{qC_r} equilibrium includes an electron transfer step and involves species with different redox-potentials. CV not only allows a characterization of the components of a solution. Relevant data can be obtained in short periods of time and with minor amounts of material (0.02 mmol).

Our previous studies showed that thiourea **L1**^[10] and squaramide **L2**^[11] (Scheme 1) are suitable additives for the bulk electrolysis of $[\text{Cp}_2\text{Ti(IV)Cl}_2]$ in THF and the use of the resulting solutions for radical arylation. The CVs (**L1**: Figure 1; **L2**: Figure 2) highlight the reasons for this assessment. Compared to the CV of $[\text{Cp}_2\text{Ti(IV)Cl}_2]$ without additives (black traces), the oxidation waves pertaining to $[\text{Cp}_2\text{Ti(III)Cl}_2]^-$ have a reduced intensity and that of $[\text{Cp}_2\text{Ti(III)Cl}]$ an increased intensity. This effect is significantly more pronounced for **L2** than for **L1**. We assumed that these effects predict a successful bulk electrolysis and catalytic radical arylation.

Encouraged by these successes, we extended the screening to the bisulfonamide **L3** (Scheme 2).^[12] The CVs (Figure 3)

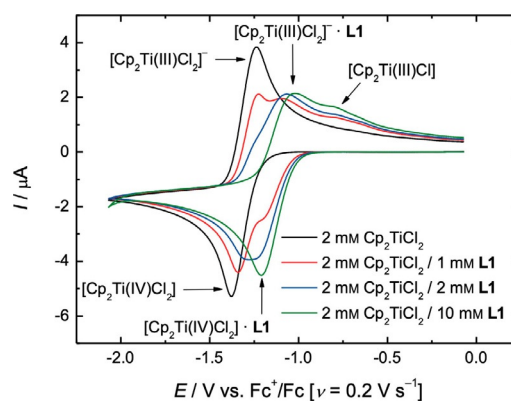


Figure 1. CVs of 2 mM Cp_2TiCl_2 and **L1** in 0.2 M $\text{Bu}_4\text{NPF}_6/\text{THF}$ at 0.2 V s^{-1} .

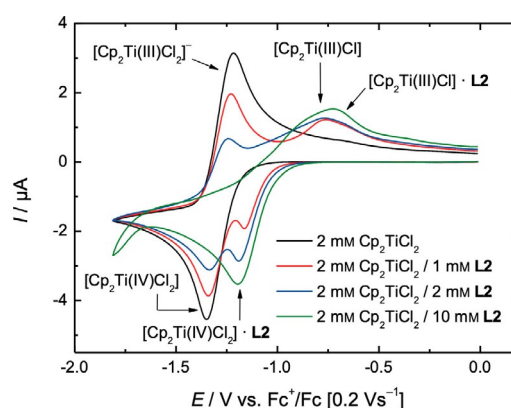
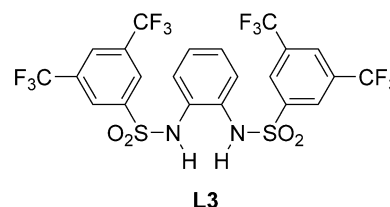


Figure 2. CVs of 2 mM Cp_2TiCl_2 and **L2** in 0.2 M $\text{Bu}_4\text{NPF}_6/\text{THF}$ at 0.2 V s^{-1} .



Scheme 2. H-bonding anion receptor **L3** investigated as additive to amplify the E_{qC_r} mechanism of Cp_2TiCl_2 .

demonstrate that the wave originating from $[\text{Cp}_2\text{Ti(III)Cl}]$ is visible. This predicts that addition of **L3** results in an efficient bulk electrolysis and a successful radical arylation (Table 1).

The performance of the epoxide arylation^[7] with **1** and 10 mol% electrochemically reduced Cp_2TiCl_2 in the presence of 1 equiv. of **L1–L3** with respect to Cp_2TiCl_2 is summarized in Table 1. In agreement with the lowest amount of $[\text{Cp}_2\text{Ti(III)Cl}]$ observed in the CV-screening, **L1** leads to the slowest reaction and lowest yield of **2**. **L2** and **L3** lead to a more active catalytic system giving essentially identical results after 2 h.

Besides their usefulness as predictors, the CVs highlight an interesting complexity of interactions between **L1–L3** and the

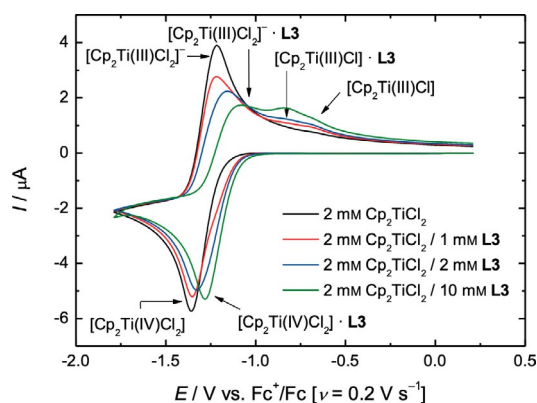


Figure 3. CVs of 2 mM Cp_2TiCl_2 and L3 in 0.2 M $\text{Bu}_4\text{NPF}_6/\text{THF}$ at 0.2 V s^{-1} .

| Table 1. Results of the arylation reaction after electrochemical activation in THF with Cp_2TiCl_2 as precatalyst and L1–L3 as additives. | |
|-----------------------------------------------------------------------------------------------------------------------------------------------------------|------------------------|
| | |
| <p>L1 2 h, 59%</p> | <p>L2 2 h, 87%</p> |
| <p>L3 2 h, 86% 4 h, 93% 5 h, 92%</p> | |
| Reaction conditions: Catalyst Cp_2TiCl_2 , additive L, 10 mM in THF, isolated yields. | |

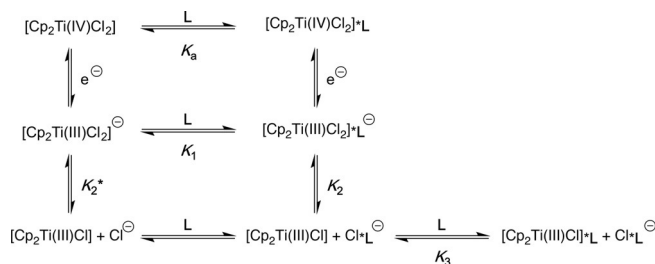
titanocene species. On the reductive sweep (the lower trace) all ligands L form an adduct with $[\text{Cp}_2\text{Ti(IV)Cl}_2]$. This adduct has a more positive reduction potential with L1 and L2 (+160 mV) showing a larger shift than L3 (+80 mV). These differences in the potentials indicate a different strength of the interactions. On the oxidative sweep (the upper trace), for all additives a complex $[\text{Cp}_2\text{Ti(III)Cl}_2]^- \cdot \text{L}$ can be detected. Again, the differences in the shift of the potentials are significant. Interestingly, only L2 and L3 seem to form complexes of the type $[\text{Cp}_2\text{Ti(III)Cl}_2] \cdot \text{L}$. The shift of the potentials relative to $[\text{Cp}_2\text{Ti(III)Cl}_2]$ suggest an electron-donating interaction for L3 (–120 mV) and an electron-withdrawing interaction for L2 (+110 mV).

Studies at the rotating ring-disk electrode

Our CV experiments are an ideal tool for the rapid screening of the additives. For a quantitative analysis, CV merely allows the direct extraction of the redox potentials of the species detected and their diffusion coefficients. More complex information on pre-equilibria or follow-up reactions can only be obtained via simulation. One general shortcoming of simulation is that, frequently, several models fit the experimental data. This is especially true for situations involving several steps and a large variety of fitting parameters. We decided to provide quantitative data for our qualitative observations made by CV. To this end, we used the rotating ring-disk electrode (RRDE).^[8] This allows assessing the results of future screening experiments on a more solid mechanistic basis.

The RRDE set-up offers major advantages over CV in stagnant solution. In CV, asymmetrically shaped current waves are observed. Therefore, “real” systems cannot be fitted to a physical equation. With a RRDE set-up this becomes possible as convection results in a time-independent and well-defined thickness of the Nernstian diffusion layer. It is composed of a disk and a ring electrode surrounding the disk. Rotation ensures a steady flow of reactants from the bulk solution to the disk. From here, the electrolyte is radially forced out to the ring and the species generated at the disk can be detected with a theoretical collection efficiency N_0 . They can be discerned by their individual redox potentials. The currents measured due to their electrochemical reactions are proportional to their concentration at the electrode surfaces and allow quantitative analysis of the composition of the solution. For potentials negative of the equilibrium of a reduction at the disk, the currents reach a plateau representing the diffusion limited current i_{lim} and can be evaluated by the Levich equation (see Supporting Information).^[13]

We started our RRDE measurements of Cp_2TiCl_2 in THF with 0.2 M NBu_4PF_6 (TBAPF₆). The data are in agreement with results of the Daasbjerg group^[4c–e] by means of CV simulation (see Supporting Information) and show that RRDE measurements are well suited for analyzing electrochemical systems based on Cp_2TiCl_2 . Based on Daasbjerg’s work we propose an extended mesh-scheme for the species present in solutions of Cp_2TiCl_2 and our additives L (Scheme 3). The monomer–dimer equilibrium of $[\text{Cp}_2\text{Ti(III)Cl}]$ is not observed in CVs with L and thus not relevant here.



Scheme 3. Proposed mesh-scheme for the $\text{Cp}_2\text{TiCl}_2/\text{L}$ redox system (L = L1, L2 or L3).

The RRDE measurements will provide the equilibrium constants given in Scheme 3 and an estimate of the solution composition before and after reduction. We will discuss the experimental results for sulfonamide **L3** and summarize the data for **L1–L3** (detailed discussion see Supporting Information).

The stabilizing effect of **L3** on $[\text{Cp}_2\text{Ti(III)Cl}_2]^-$ can be observed directly from the positive shift of the voltammograms detected at the disk i_D and the decreasing transfer ratios ($i_R/i_D/N_0$) for measurements with Cp_2TiCl_2 and **L3** at a rotation frequency f of 25 Hz and a ring potential E_R of 0.05 V (Figure 4, for measurements at $f = 4$ Hz and $E_R = 0.23, 0.42$ and 0.66 V see Supporting Information). A potential of 0.05 V vs. Ag/Ag^+ solely allows the oxidation of $[\text{Cp}_2\text{Ti(III)Cl}_2]^-$ (Figure 3, please note that the Fc^+/Fc scale is shifted by ca. -1.1 V). Thus, only this species is detected at the ring.

L3 (10 mM, 5.0 equiv.) leads to a positive shift of the reduction potential and a slight decrease of i_D in the diffusion limited region at the disk electrode from -1.54 mA cm^{-2} to -1.46 mA cm^{-2} (Figure 4a) and to a significant decrease of the normalized ring current i_R/N_0 by a factor of 4 (Figure 4b). The transfer ratio, which is directly proportional to the concentration of $[\text{Cp}_2\text{Ti(III)Cl}_2]^-$ in solution (Figure 4c), decreases from 0.85 in the base electrolyte to 0.18 when adding 10 mM (5.0 equiv.) **L3**.

L3 (1 mM, 0.5 equiv.) leads to the formation of a shoulder in the disk current at -0.05 V (Figure 4a), which allows us to obtain equilibrium constant K_a (Scheme 3). The decreased diffusion-limited current at the disk indicates a reaction of $[\text{Cp}_2\text{Ti(IV)Cl}_2]$ with **L3** to $[\text{Cp}_2\text{Ti(IV)Cl}_2] \cdot \text{L3}$ associated with a change of the diffusion coefficient prior to the electrochemical reaction. If the reaction of **L3** occurred after the electrochemical reduction of $[\text{Cp}_2\text{Ti(IV)Cl}_2]$, this should not have an impact on the diffusion-limited current.

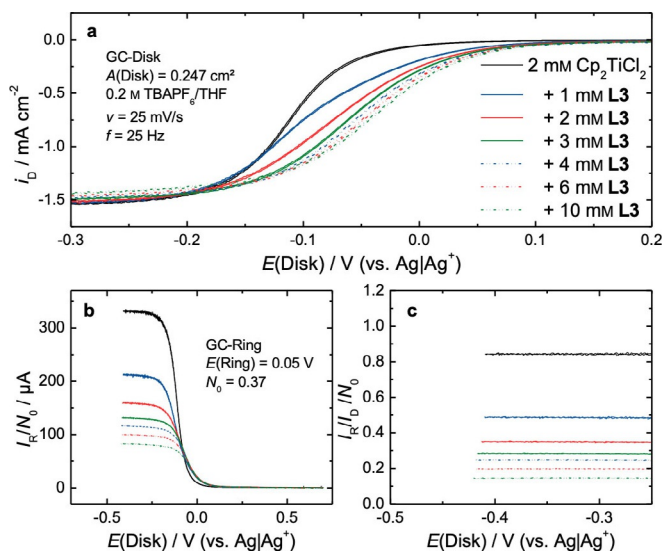


Figure 4. Disk current densities i_D (a), normalized ring currents i_R/N_0 (b) and transfer ratios $i_R/i_D/N_0$ (c) of the RRDE measurements of a solution of 2 mM Cp_2TiCl_2 in 0.2 M $\text{NBu}_4\text{PF}_6/\text{THF}$ with different concentrations of **L3** at a ring potential E_R of 0.05 V and a rotation frequency f of 25 Hz.

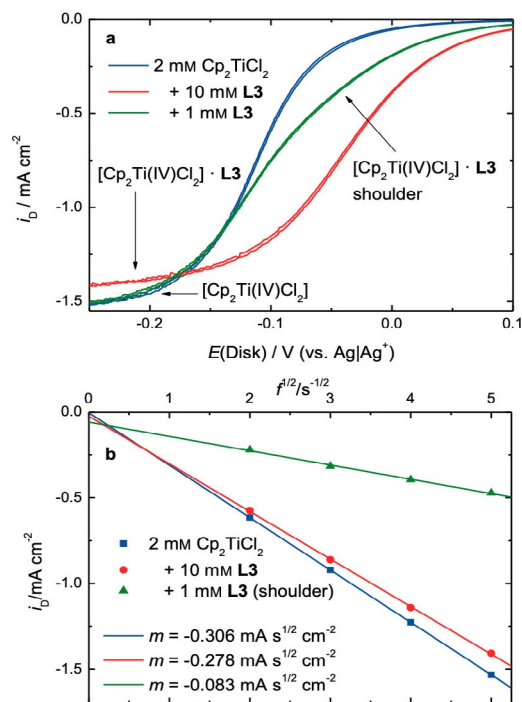


Figure 5. Cut-out of the RDE measurements shown in Figure 4a (a) highlighting the shoulder in the 1 mM **L3** measurement and diffusion limited current densities (b) at the disk i_D as a function of $f^{1/2}$ for Cp_2TiCl_2 and with 10 mM of **L3** or 1 mM of **L3** (shoulder). The slopes of the linear fits are given as m .

According to the Levich equation, the limiting current density at the disk electrode is proportional to $D^{2/3}$ (D : diffusion coefficient) and to $f^{1/2}$. Figure 5b depicts the diffusion-limited i_D of $[\text{Cp}_2\text{Ti(IV)Cl}_2]$ and with 10 mM of **L3** alongside the shoulder current density found for the measurement of **L3** (1 mM, 0.5 equiv.) as a function of $f^{1/2}$. The graphical representation of the data yields straight lines. The non-zero intercept of the line representing the shoulder currents indicates that the current flow is not solely limited by diffusion. Possibly the kinetics of the reduction of the unbound species already play a minor role. We assume that in the solutions with 10 mM of **L3** approximately all $[\text{Cp}_2\text{Ti(IV)Cl}_2]$ is bound to **L3**. The different slopes observed for the experiments with base electrolyte and with 10 mM **L3** yield the ratio of the diffusion coefficients of $[\text{Cp}_2\text{Ti(IV)Cl}_2]$ and $[\text{Cp}_2\text{Ti(IV)Cl}_2] \cdot \text{L3}$ according to the Levich equation. The diffusion coefficient D of $[\text{Cp}_2\text{Ti(IV)Cl}_2]$ is 1.15 times larger than that of $[\text{Cp}_2\text{Ti(IV)Cl}_2] \cdot \text{L3}$ (1.15 with **L1** and 1.33 with **L2**). In the measurement with 1 mM **L3** the diffusion-limited reduction of $[\text{Cp}_2\text{Ti(IV)Cl}_2] \cdot \text{L3}$ is observed as a shoulder prior to the reduction of $[\text{Cp}_2\text{Ti(IV)Cl}_2]$, as the reaction between $[\text{Cp}_2\text{Ti(IV)Cl}_2]$ and **L3** is incomplete. From the ratio of this shoulder to the subsequent plateau, the equilibrium constant of association K_a of **L3** to $[\text{Cp}_2\text{Ti(IV)Cl}_2]$ is accessible. With a value of 1.07 mM^{-1} , **L3** lies between **L1** (0.69 mM^{-1}) and **L2** (1.81 mM^{-1}).

We studied the composition of the reduced solutions of Ti^{III} to obtain K_1 to K_3 (Scheme 3) by analyzing the effect of **L** on the transfer ratios (compare Figure 4c). The fixed ring potential E_R allows the detection of all species that can be oxidized up

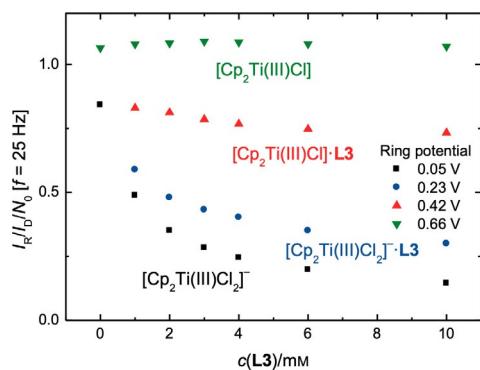


Figure 6. Transfer ratios $I_R/I_D/N_0$ for the measurements of Cp_2TiCl_2 and **L3** at different concentrations of **L3** at ring potentials of 0.05, 0.23, 0.42 and 0.66 V and at a rotation frequency f of 25 Hz.

to this potential. The step-wise increase of E_R afforded transfer ratios for $[\text{Cp}_2\text{Ti}(\text{III})\text{Cl}_2]^-$, $[\text{Cp}_2\text{Ti}(\text{III})\text{Cl}_2]^-*\text{L3}$, $[\text{Cp}_2\text{Ti}(\text{III})\text{Cl}]$ and $[\text{Cp}_2\text{Ti}(\text{III})\text{Cl}]*\text{L3}$. These transfer ratios are shown in Figure 6 as a function of the concentration of **L3**.

The transfer ratios allow the calculation of the equilibrium constants between the Ti^{III} species (see Supporting Information for details). The association equilibrium constant K_1 of **L3** to $[\text{Cp}_2\text{Ti}(\text{III})\text{Cl}_2]^-$ amounts to 0.4 mM^{-1} (2 mM^{-1} for **L1**, 0.3 mM^{-1} for **L2**). Dissociation of $\text{Cl}^-*\text{L3}$ from $[\text{Cp}_2\text{Ti}(\text{III})\text{Cl}_2]^-*\text{L3}$ has an equilibrium constant K_2 of 3.0 mM (2.8 mM for **L1**, 54 mM for **L2**). The formation of $[\text{Cp}_2\text{Ti}(\text{III})\text{Cl}]*\text{L3}$ has a K_3 of 0.7 mM^{-1} (0.5 mM^{-1} for **L2**). This adduct is not observed for **L1**.

For these equilibria we have assumed the formation of 1:1 adducts. The concentration-dependent measurements can verify this assumption. The voltammograms of i_D (Figure 4a) show a gradual shift of the reduction potential starting from a concentration of 2 mM of **L3**. This implies that the Nernst equation for this redox process depends on the concentration of free **L3**. When plotting the half-wave potential $E_{1/2}$ against the decadic logarithm of the concentration of **L3** (Figure 7) a linear relation with a slope m of roughly 60 mV dec^{-1} at all rotation frequencies is obtained.

Therefore, the Nernst equation for this redox system must be linearly dependent on $\log(c(\text{L3})^p)$ with p representing the

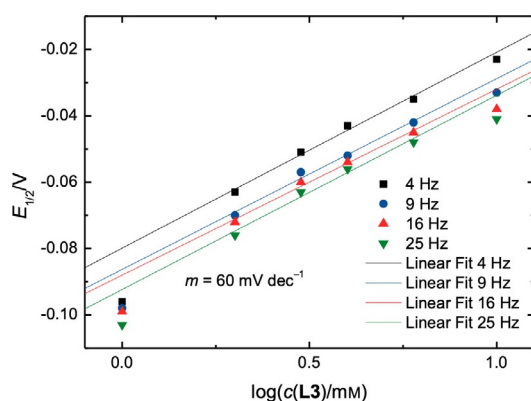


Figure 7. Plots of the half-wave potential $E_{1/2}$ of the RRDE measurements with Cp_2TiCl_2 and **L3** as a function of the decadic logarithm of the concentration of **L3**.

number of **L3** ligands attached to the titanocene.^[14] With **L1** the same slope of 60 mV dec^{-1} was obtained showing that p is equal to 1. This verifies our initial assumption. The mechanisms of chloride abstraction from the Ti^{III} complexes and activation of the Ti^{IV} complexes are likely to be similar for **L1** and **L3**.

For **L2** a slope of 30 mV dec^{-1} was observed (Figure 8). Thus, the redox potential is proportional to $\log(c(\text{L2})^q)$ and $q = p/2$. Thus, we propose the reversible formation of a 2:1 adduct between $[\text{Cp}_2\text{Ti}(\text{III})\text{Cl}]$ and **L2** in addition to the equilibria shown in Scheme 3. For the case that only this 2:1 adduct formation between $[\text{Cp}_2\text{Ti}(\text{III})\text{Cl}]$ and **L2** is considered (in contrast to the 1:1 adduct considered for K_1 to K_3 given above) a new set of equilibrium constants for the Ti^{III} species has to be calculated ($K_1' = 0.2 \text{ mM}^{-1}$, $K_2' = 54 \text{ mM}$, $K_3' = 0.1 \text{ mM}^{-2}$). However, it is likely that both adducts are present in the reduced solutions.

The equilibrium constants obtained from the RRDE-studies together with the relative amounts of the relevant Ti^{IV} (in red) and Ti^{III} species (in green) at concentrations of 2 mM in **Ti** and **L** are summarized in Scheme 4. $[\text{Cp}_2\text{Ti}(\text{IV})\text{Cl}_2]$ is complexed in

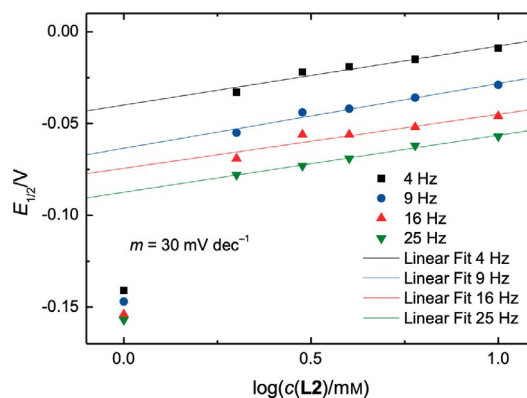
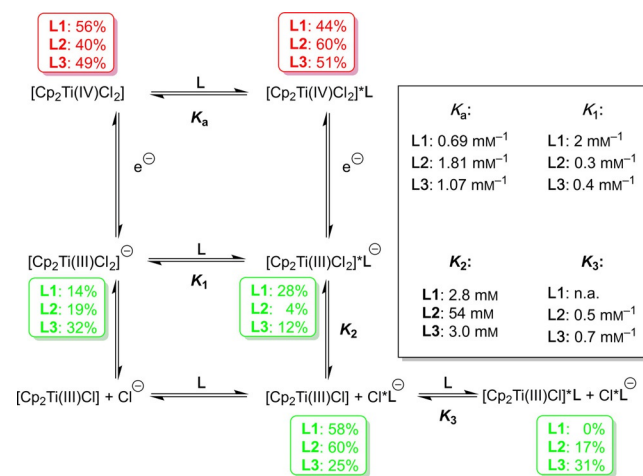


Figure 8. Plots of the half-wave potential $E_{1/2}$ of the RRDE measurements with Cp_2TiCl_2 and **L2** as a function of the decadic logarithm of the concentration of **L2**.



Scheme 4. Mesh-scheme for the $\text{Cp}_2\text{TiCl}_2/\text{L}$ redox system ($\text{L} = \text{L1, L2}$ or **L3**) including the equilibrium constants obtained in the RRDE measurements and the solution composition in % $[\text{Ti}^{\text{IV}}]$ (in red, Ti^{III} in green).

40%–60% amounts (red numbers) by **L1**–**L3** with **L2** being slightly more efficient than the other additives as indicated by the K_a values.

The additives **L1**–**L3** have a stronger influence on the equilibria involving $[\text{Cp}_2\text{Ti(III)Cl}]$. In the presence of **L2**, essentially no $[\text{Cp}_2\text{Ti(III)Cl}_2]^- * \text{L2}$ is formed because **L2** binds Cl^- too strongly. Interestingly, **L2** complexes $[\text{Cp}_2\text{Ti(III)Cl}]$ less efficiently than **L3** whereas **L1** forms no $[\text{Cp}_2\text{Ti(III)Cl}] * \text{L1}$. As a result, the use of **L2** results in the highest combined relative amount (77%) of the catalytically active $[\text{Cp}_2\text{Ti(III)Cl}]$ and $[\text{Cp}_2\text{Ti(III)Cl}] * \text{L2}$. For **L1** and **L3**, the solution contains relatively high proportions of $[\text{Cp}_2\text{Ti(III)Cl}_2]^- * \text{L}$ and $[\text{Cp}_2\text{Ti(III)Cl}_2]^-$ that constitute the resting state of the active catalyst. This situation may be advantageous when catalyst stability is more important than catalyst activity.

The RRDE investigations underline that our use of the E_{qC_r} equilibrium as predictor for the performance of the bulk electrolysis of Cp_2TiCl_2 in THF as well as for the titanocene catalyzed radical arylation of epoxides has a sound mechanistic basis. Moreover, the quantitative data obtained allow an accurate prediction of the composition of an electrochemically reduced solution of Cp_2TiCl_2 containing additives that is essential for a precise control of the reaction conditions. This may be essential for applications on large scale.

Density functional theory studies

To relate the data obtained from RRDE and CV measurements to molecular properties, we studied the structures and energies of the species involved in the E_{qC_r} equilibrium by DFT methods. The Grimme group has recently developed a powerful multilevel approach to address such situations. It consists of the CREST code^[15] for searching the low-energy chemical space by tight-binding semi-empirical theory based *meta*-dynamics (MTD) calculations (see Ref. [16]). The resulting conformer ensemble is refined efficiently in multiple DFT steps with the ENSO code^[17] as a driver for ORCA or TURBOMOLE quantum chemistry packages.^[18] For a recent overview of the main xTB code used for the GFN tight-binding or force field calculations see Ref. [19].

Accordingly, we used the xTB, CREST and ENSO programs to determine the structures with the lowest free energy in THF solution for each ligand **L** and all complexes. These calculations were conducted in the same workflow. Manually prepared starting structures, which are initially preoptimized with the GFN2-xTB[GBSA] tight binding model are used in the CREST program that employs MTD at the same level in order to obtain a relative complete ensemble of likely structures. The ENSO program determines the equilibrium (Boltzmann) populations for a few low-lying conformers at higher theoretical levels in three steps. First, already relatively accurate B97-3c[DCOSMO-RS(THF)] (a composite low-cost DFT method^[20]) single point energies are calculated on the CREST ensemble. Structures within an energy threshold of 4 kcal mol⁻¹ above the lowest lying structure are then fully optimized at the same level. In this first filtering step thermostistical free energies in the modified rigid-rotor/harmonic-oscillator (mRRHO) approximation^[21] calculated with GFN2-xTB[GBSA] and the free energy

of solvation in THF calculated with the accurate COSMO-RS^[22] solvation model are added. Finally, for all structures within a 2 kcal mol⁻¹ threshold an even better single point energy is computed at the PW6B95-D3/def2-TZVPP^[23] hybrid DFT level which basically replaces the corresponding B97-3c energy. In summary, the final complete total free energy used consists of the mRRHO part from the GFN2-xTB treatment, the COSMO-RS part in THF for solvation and the basic electronic energy with the PW6B95-D3 functional. In the following, the conformer of each species with the lowest total free energy is given, if not stated otherwise.

Structures of **L** and $\text{Cl}^- * \text{L}$

We started our investigations with the ligands **L** and their chloride complexes $\text{Cl}^- * \text{L}$. As free species, **L2** shows higher conformational rigidity than **L1** and **L3** (for a detailed discussion see Supporting Information). The structures of the most stable conformers were chosen as reference points for the energies of formation of all other complexes. A potential self-aggregation of **L2** in THF is beyond the scope of this study.^[24]

The structures of the $\text{Cl}^- * \text{L}$ and energies of complexation with respect to the lowest energy conformer of the respective **L** are depicted in Figure 9. Cl^- is bound to both N–H groups of all ligands. The $\text{Cl}^- * \text{L}$ complexes with **L1** and **L2** show C_{2v} symmetry. $\text{Cl}^- * \text{L2}$ is conformationally rigid in agreement with its X-ray structure.^[25] $\text{Cl}^- * \text{L1}$ has a second conformer 4.6 kcal mol⁻¹ higher in energy than the one shown with one NHR group rotated by almost 180° and the other bound to Cl^- . A second conformer of $\text{Cl}^- * \text{L3}$ is 2.0 kcal mol⁻¹ higher in energy and has a similar structure to the one shown. In agreement with a previous study on the chloride binding of thioureas, squaramides

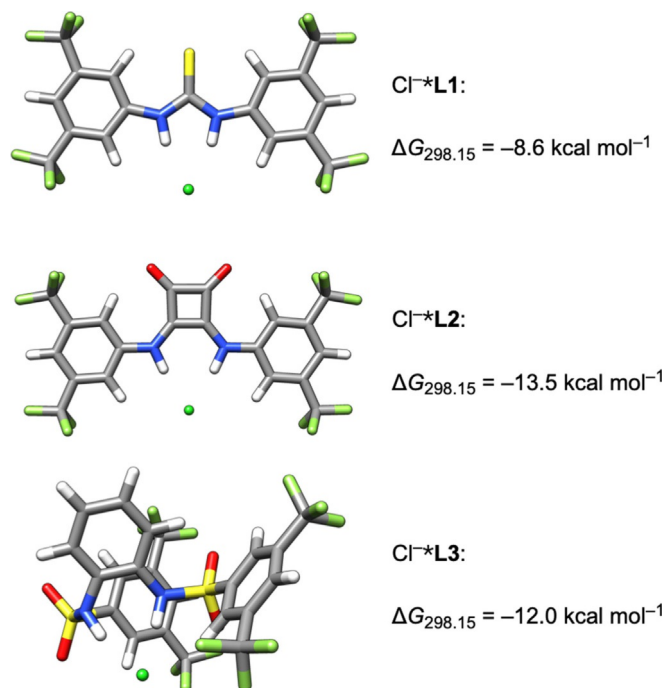


Figure 9. DFT structures of the $\text{Cl}^- * \text{L}$ adducts of **L1**, **L2** and **L3**.

and sulfonamides,^[12] $\Delta G_{298.15}$ for $\text{Cl}^- \cdot \text{L}$ show that **L2** binds chloride stronger than **L1** and **L3**. As also pointed out in that study, the strength of chloride binding does not correlate with the $\text{p}K_a$ values of the different receptors.

Supramolecular complexes of **L** and Ti^{III}

The supramolecular complexes $[\text{Cp}_2\text{Ti}(\text{III})\text{Cl}_2]^- \cdot \text{L}$ are crucial intermediates in the electrochemical generation of $[\text{Cp}_2\text{Ti}(\text{III})\text{Cl}]$ from $[\text{Cp}_2\text{Ti}(\text{IV})\text{Cl}_2]$. They provide a mechanism for shifting the $E_q C_r$ equilibrium to $[\text{Cp}_2\text{Ti}(\text{III})\text{Cl}]$ by facilitating chloride abstraction and dissolution of $[\text{Cp}_2\text{Ti}(\text{III})\text{Cl}_2]^- \cdot \text{L}$. Another intriguing aspect is that binding of **L** to $[\text{Cp}_2\text{Ti}(\text{III})\text{Cl}]$ directly impacts the redox properties of $[\text{Ti}]$ in the arylation reaction.

The structures of $[\text{Cp}_2\text{Ti}(\text{III})\text{Cl}_2]^- \cdot \text{L}$ together with the corresponding values for $\Delta G_{298.15}$ and $\Delta H_{298.15}$ are depicted in Figure 10 and reveal that **L1** and **L2** bind both chloride ligands with the N–H groups, providing complexes that are C_2 -symmetric within the limits of accuracy. This is exemplified by the

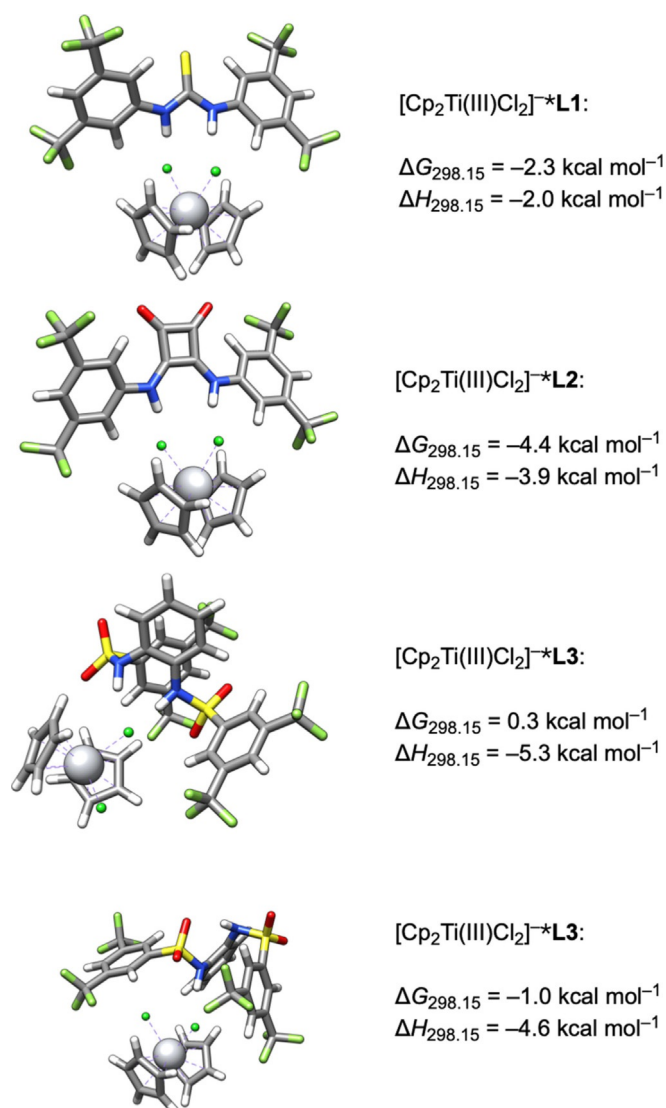


Figure 10. DFT structures of the $[\text{Cp}_2\text{Ti}(\text{III})\text{Cl}_2]^- \cdot \text{L}$ adducts of **L1**, **L2** and **L3**.

$\text{Ti}-\text{Cl}$ bond lengths ($[\text{Cp}_2\text{Ti}(\text{III})\text{Cl}_2]^- \cdot \text{L1}$: 2.545 Å and 2.540 Å, $[\text{Cp}_2\text{Ti}(\text{III})\text{Cl}_2]^- \cdot \text{L2}$: 2.547 Å and 2.550 Å).

Curiously, for **L3** a binding of both N–H groups was not observed. In the more stable complex (Figure 10, lowest structure) **L3** only binds to one of the chloride ligands with one N–H group ($\text{Ti}-\text{Cl}$ bond lengths: 2.53 Å and 2.50 Å). In the second most stable complex (3rd structure from the top of Figure 10), both N–H groups coordinate to one chloride in a “side-on” geometry. This results in distinctly different $\text{Ti}-\text{Cl}$ bond lengths (2.59 Å and 2.49 Å). Enthalpically, the less stable complex is slightly favored ($\Delta H_{298.15} = -5.3$ vs. $-4.6 \text{ kcal mol}^{-1}$). However, the entropically disfavored restriction of conformational freedom in this binding mode is the more relevant contribution to $\Delta G_{298.15}$. According to the values for $\Delta G_{298.15}$, the binding via both N–H and $\text{Ti}-\text{Cl}$ groups by **L1** and **L2** results in a stronger binding of $[\text{Cp}_2\text{Ti}(\text{III})\text{Cl}_2]^-$.

According to the CV and RRDE measurements, **L1** does not bind to $[\text{Cp}_2\text{Ti}(\text{III})\text{Cl}]$ whereas both **L2** and **L3** do. However, they bind in a different fashion as evident from the shifted oxidation potentials for $[\text{Cp}_2\text{Ti}(\text{III})\text{Cl}] \cdot \text{L}$ (**L2**: +110 mV, **L3**: –120 mV). We analyzed the complex formation starting from $[\text{Cp}_2\text{Ti}(\text{III})\text{Cl}]$ and **L** and included the effect of additional coordination with THF (Figure 11, also see Supporting Information).

L1 and **L2** display a similar complexation behavior. Adduct formation is substantially more favorable with $[\text{Cp}_2\text{Ti}(\text{III})\text{Cl}](\text{THF})$. As for $[\text{Cp}_2\text{Ti}(\text{III})\text{Cl}_2]^-$ both additives bind the

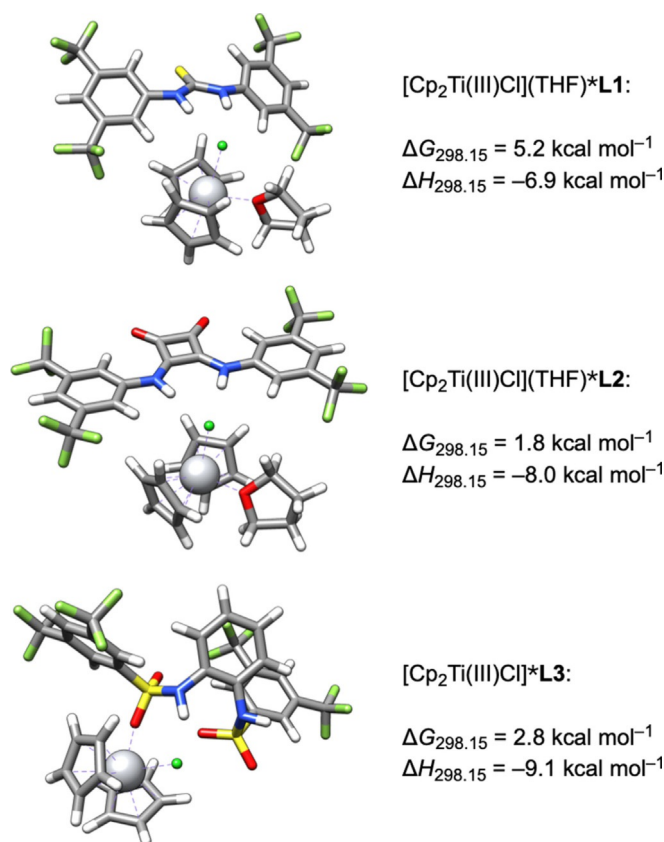


Figure 11. DFT structures of the $[\text{Cp}_2\text{Ti}(\text{III})\text{Cl}](\text{THF}) \cdot \text{L}$ adducts of **L1** and **L2** and of $[\text{Cp}_2\text{Ti}(\text{III})\text{Cl}] \cdot \text{L3}$.

chloride ligand with both N–H groups. Adduct formation is disfavored with **L1**. This is in agreement with the experiment, where no $[\text{Cp}_2\text{Ti(III)Cl}]\cdot\text{L1}$ was observed. The interaction of **L2** with the chloride ligand leads to an increase of the Ti–Cl bond length by 0.13 Å. This is in agreement with the experimentally observed positive shift of the redox potential.

The situation is different for **L3**. The favored complexation mode is realized with $[\text{Cp}_2\text{Ti(III)Cl}]$ as starting material. This is due to an intramolecular interaction of one of the sulfonamide groups with Ti that renders an additional complexation of THF superfluous. The coordination of the sulfonamide increases the electron density at Ti in agreement with the experimentally observed negative shift in the redox potential for $[\text{Cp}_2\text{Ti(III)Cl}]\cdot\text{L3}$. Only the adjacent N–H group binds to the chloride ligand.

The slope of 30 mV dec^{-1} in the RRDE measurements with **L2** (Figure 8) suggests that a 2:1 stoichiometry of $[\text{Cp}_2\text{Ti(III)Cl}]$ and **L2** in the adduct formation is possible. The computed structure of the 2:1 complex with one molecule of THF and its $\Delta G_{298.15}$ and $\Delta H_{298.15}$ with respect to the dissociated species are depicted in Figure 12. Complex formation without THF is distinctly less favorable.

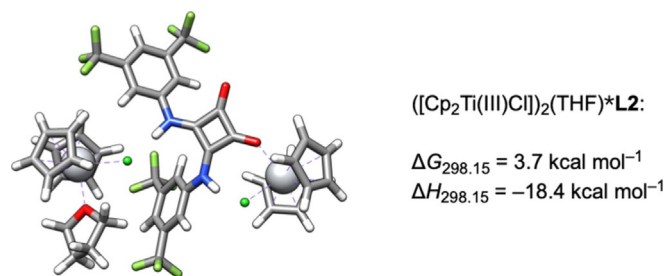


Figure 12. DFT structure of the $([\text{Cp}_2\text{Ti(III)Cl}])_2(\text{THF})\cdot\text{L2}$ adduct.

Enthalpically, complex formation is strongly favored and the slightly positive $\Delta G_{298.15}$ is due to the entropically disadvantageous formation of the complex from four components.

L2 binds the second titanocene through one of the carbonyl oxygens. At the same time, the N–H groups each bind to one of the chloride ligands of both titanocenes. This makes **L2** a bifunctional ligand and provides an explanation for the broad oxidation wave in the area of Cp_2TiCl found in CVs of Cp_2TiCl_2 and **L2**. On the oxidative sweep $([\text{Cp}_2\text{Ti(III)Cl}])_2\cdot\text{L2}$ is oxidized first followed by $[\text{Cp}_2\text{Ti(III)Cl}]$ and finally $[\text{Cp}_2\text{Ti(III)Cl}]\cdot\text{L2}$.

Supramolecular complexes of L and Ti^{IV}

Finally, we investigated the adduct formation between $[\text{Cp}_2\text{Ti(IV)Cl}_2]$ and **L**. This pre-equilibrium to the E_{qC} mechanism allows the use of a less negative reduction potential in bulk electrolysis (–1.3 V vs. Ag/Ag^+ with **L2**, –1.4 V with **L1** and **L3**). Figure 13 shows the structures of the hydrogen bonded adducts between $[\text{Cp}_2\text{Ti(IV)Cl}_2]$ and **L1–L3**. For **L2**, the minimum structure of $[\text{Cp}_2\text{Ti(IV)Cl}_2]\cdot\text{L2}$ is a van der Waals complex that is 0.3 kcal mol^{-1} more stable than the complex shown (see

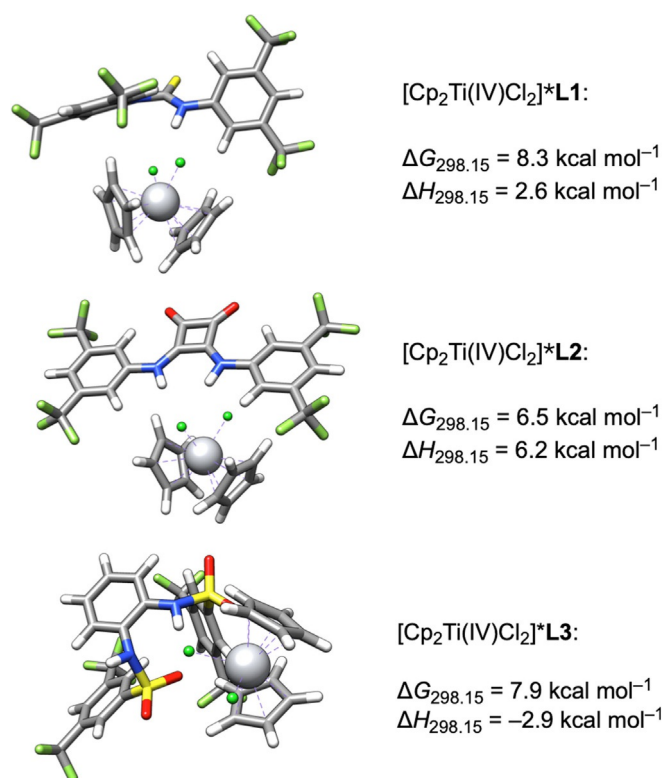


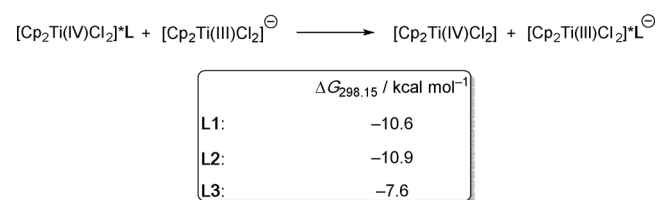
Figure 13. DFT structures of the $[\text{Cp}_2\text{Ti(IV)Cl}_2]\cdot\text{L}$ adducts of **L1**, **L2** and **L3**.

Supporting Information for details). It is not discussed here, as it does not suggest a positive shift of the reduction potential.

Compared to the complexes of $[\text{Cp}_2\text{Ti(III)Cl}_2]\cdot\text{L}$ the formation of the adducts of $[\text{Cp}_2\text{Ti(IV)Cl}_2]\cdot\text{L}$ is less favorable. The calculated structures show that with the neutral Ti^{IV} complex only **L2** can interact with both N–H groups. However, they both bind to the same chloride ligand. In the adducts of **L1** and **L3** only one of the N–H groups is coordinating chloride, the other is pointing away from the complex resulting in a noticeable conformational change of the additive.

The computed order of stability of the adducts is in agreement with the stronger binding affinity of **L2** to $[\text{Cp}_2\text{Ti(IV)Cl}_2]$ observed in the RRDE measurements.

The lower stability of $[\text{Cp}_2\text{Ti(IV)Cl}_2]\cdot\text{L}$ compared to $[\text{Cp}_2\text{Ti(III)Cl}_2]\cdot\text{L}$ is most easily rationalized by the negative charge in $[\text{Cp}_2\text{Ti(III)Cl}_2]^-$ that renders hydrogen bonding more attractive because of the coulomb attraction. We investigated this point by analyzing the exchange reactions shown in Scheme 5. The effect of the charge is indeed substantial as



Scheme 5. Gibbs energies of the exchange reaction between $[\text{Cp}_2\text{Ti(IV)Cl}_2]\cdot\text{L}$ and $[\text{Cp}_2\text{Ti(III)Cl}_2]^-$.

highlighted by the highly exergonic formation of the $[\text{Cp}_2\text{Ti(III)Cl}_2]^{-*}\text{L}$ adducts from their $[\text{Cp}_2\text{Ti(IV)Cl}_2]^{*}\text{L}$ counterparts.

Conclusions

In summary, we have demonstrated that our approach of screening the E_{qC} equilibrium as predictor for the bulk electrolysis of Cp_2TiCl_2 in THF and the titanocene catalyzed radical arylation of epoxides has a sound mechanistic basis. This was achieved by a combination of synthesis, the application of the electrochemical techniques cyclic voltammetry (CV) and rotating ring-disk electrode (RRDE) measurements, as well as DFT investigations.

We have introduced bisulfonamides as additives for enabling bulk electrolysis of Cp_2TiCl_2 in THF as well as for the titanocene catalyzed radical arylation of epoxides. For the first time, we have provided quantitative data about the E_{qC} equilibrium in the presence of a thiourea, a squaramide and a bisulfonamide and have established the stoichiometry of adduct formations between $[\text{Cp}_2\text{Ti(III)Cl}_2]^{-}$, $[\text{Cp}_2\text{Ti(III)Cl}]$ and $[\text{Cp}_2\text{Ti(IV)Cl}_2]$. By studying the complexes by DFT methods, we have provided the Gibbs energies and enthalpies of complexation as well as the adduct structures. Our studies show that a balance between activity and stability of the catalyst are vital for reaction efficiency. Changing the inorganic ligand of Cp_2TiX_2 was not investigated here. Previous investigations^[5] have shown that for Cp_2TiBr_2 derived catalysts halide abstraction is easier than for complexes derived from Cp_2TiCl_2 . The intricate interactions between the additives and the titanocenes by hydrogen bonding and coordination of polar groups are not only in agreement with the electrochemical data. They also provide a design platform for the development of novel additives for catalysis in single electron steps^[26] or metalloradical catalysis^[27] in particular in enantioselective catalysis.

Acknowledgements

We thank the DFG (Ga 619/13-1), the "Jürgen Manchot Stiftung" (T.H.), the "Studienstiftung des deutschen Volkes" (S.K. and P.H.R.), and the "Evangelisches Studienwerk Villigst" (T.L.) Open access funding enabled and organized by Projekt DEAL.

Conflict of interest

The authors declare no conflict of interest.

Keywords: catalysis · density functional calculations · electrochemistry · radicals · screening

- [1] a) P. T. Anastas, M. M. Kirchhoff, *Acc. Chem. Res.* **2002**, *35*, 686–694; b) Efficient screening processes are essential for green chemistry approaches, see: C. W. Coley, N. S. Eyke, K. F. Jensen, *Angew. Chem. Int. Ed.* **2020**, <https://doi.org/10.1002/anie.201909987>, *Angew. Chem.* **2020**, <https://doi.org/10.1002/ange.201909987>; c) C. W. Coley, N. S. Eyke, K. F. Jensen, *Angew. Chem. Int. Ed.* **2020**, <https://doi.org/10.1002/anie.201909989> *Angew. Chem.* **2020**, <https://doi.org/10.1002/ange.201909989>; d) S. Ahn, M. Hong, M. Sundararajan, D. H. Ess, M.-H. Baik, *Chem. Rev.* **2019**, *119*, 6509–6560; e) for selected examples see: M. N. Hopkinson, A. Gómez-Suárez, M. Teders, B. Sahoo, F. Glorius, *Angew. Chem. Int. Ed.* **2016**, *55*, 4361–4366; *Angew. Chem.* **2016**, *128*, 4434–4439; f) M. Teders, A. Gómez-Suárez, L. Pitzer, M. N. Hopkinson, F. Glorius, *Angew. Chem. Int. Ed.* **2017**, *56*, 902–906; *Angew. Chem.* **2017**, *129*, 921–925.

- [2] a) A. Gansäuer, A. Fleckhaus, M. Alejandro Lafont, A. Okkel, K. Kotsis, A. Anoop, F. Neese, *J. Am. Chem. Soc.* **2009**, *131*, 16989–16999; b) A. Gansäuer, S. Hildebrandt, E. Vogelsang, R. A. Flowers II, *Dalton Trans.* **2016**, *45*, 448–452.
- [3] J. I. van der Vlugt, *Chem. Eur. J.* **2019**, *25*, 2651–2662.
- [4] a) Y. Mugnier, C. Moise, E. Laviron, *J. Organomet. Chem.* **1981**, *204*, 61–66; b) E. Samuel, J. Vedel, *Organometallics* **1989**, *8*, 237–241; c) R. J. Enemærke, J. Larsen, T. Skrydstrup, K. Daasbjerg, *Organometallics* **2004**, *23*, 1866–1874; d) R. J. Enemærke, J. Larsen, T. Skrydstrup, K. Daasbjerg, *J. Am. Chem. Soc.* **2004**, *126*, 7853–7864; e) R. J. Enemærke, J. Larsen, G. H. Hjöllund, T. Skrydstrup, K. Daasbjerg, *Organometallics* **2005**, *24*, 1252–1262.
- [5] CV-Screening: a) T. Liedtke, P. Spanning, L. Riccardi, A. Gansäuer, *Angew. Chem. Int. Ed.* **2018**, *57*, 5006–5010; *Angew. Chem.* **2018**, *130*, 5100–5104; b) T. Liedtke, T. Hilche, S. Klare, A. Gansäuer, *ChemSusChem* **2019**, *12*, 3166–3171.
- [6] Arylation: a) P. Wipf, J. P. Maciejewski, *Org. Lett.* **2008**, *10*, 4383–4386; b) A. Gansäuer, M. Behlendorf, D. von Laufenberg, A. Fleckhaus, C. Kube, D. V. Sadasivam, R. A. Flowers II, *Angew. Chem. Int. Ed.* **2012**, *51*, 4739–4742; *Angew. Chem.* **2012**, *124*, 4819–4823; c) A. Gansäuer, C. Kube, K. Daasbjerg, R. Sure, S. Grimme, G. D. Fianu, D. V. Sadasivam, R. A. Flowers II, *J. Am. Chem. Soc.* **2014**, *136*, 1663–1671; d) A. Gansäuer, D. von Laufenberg, C. Kube, T. Dahmen, A. Michelmann, M. Behlendorf, R. Sure, M. Seddiqzai, S. Grimme, D. V. Sadasivam, G. D. Fianu, R. A. Flowers II, *Chem. Eur. J.* **2015**, *21*, 280–289; e) A. Gansäuer, S. Hildebrandt, A. Michelmann, T. Dahmen, D. von Laufenberg, C. Kube, G. D. Fianu, R. A. Flowers II, *Angew. Chem. Int. Ed.* **2015**, *54*, 7003–7006; *Angew. Chem.* **2015**, *127*, 7109–7112; f) R. B. Richrath, T. Olyschläger, S. Hildebrandt, D. G. Enny, G. D. Fianu, R. A. Flowers II, A. Gansäuer, *Chem. Eur. J.* **2018**, *24*, 6371–6379; g) F. Mühlhaus, H. Weißbarth, T. Dahmen, G. Schnakenburg, A. Gansäuer, *Angew. Chem. Int. Ed.* **2019**, *58*, 14208–14212; *Angew. Chem.* **2019**, *131*, 14346–14350. h) Comparison to 5-exo cyclization: A. Gansäuer, M. Seddiqzai, T. Dahmen, R. Sure, S. Grimme, *Beilstein J. Org. Chem.* **2013**, *9*, 1620–1629; i) A. Gansäuer, M. Pierobon, *Synlett* **2000**, 1357–1359.
- [7] With H_2O as supramolecular chloride binder, Cp_2Ti^+ is irreversibly formed: a) A. Gansäuer, M. Behlendorf, A. Cangönül, C. Kube, J. M. Cuerva, J. Friedrich, M. van Gastel, *Angew. Chem. Int. Ed.* **2012**, *51*, 3266–3270; *Angew. Chem.* **2012**, *124*, 3320–3324. b) For the use of this concepts with other metals see: E. P. Farney, S. J. Chapman, W. B. Swords, M. D. Torelli, R. J. Hames, T. P. Yoon, *J. Am. Chem. Soc.* **2019**, *141*, 6385–6391.
- [8] a) C. Sandford, M. A. Edwards, K. J. Klunder, D. P. Hickey, M. Li, K. Barman, M. S. Sigman, H. S. White, S. D. Minter, *Chem. Sci.* **2019**, *10*, 6404–6422; b) W. J. Albery, *Trans. Faraday Soc.* **1966**, *62*, 1915–1919; c) W. J. Albery, S. Bruckenstein, *Trans. Faraday Soc.* **1966**, *62*, 1920–1931; d) K. B. Prater, A. J. Bard, *J. Electrochem. Soc.* **1970**, *117*, 1517–1520; e) A. J. Bard, L. R. Faulkner, *Electrochemical Methods*, 2nd ed., Wiley, New York, **2001**, Chapter 9; f) W. J. Albery, M. L. Hitchman, *Ring-Disc Electrodes*, Clarendon, Oxford, **1971**.
- [9] a) A. J. Bard, L. R. Faulkner, *Electrochemical Methods: Fundamentals and Applications*, 2nd ed., Wiley, New York, **2001**; b) A. Jutand, *Chem. Rev.* **2008**, *108*, 2300–2347; c) W. E. Geiger, *Coord. Chem. Rev.* **2013**, *257*, 1459–1471.
- [10] a) A. Wittkopp, P. R. Schreiner, *Chem. Eur. J.* **2003**, *9*, 407–414; b) K. M. Lippert, K. Hof, D. Gerbig, D. Ley, H. Hausmann, S. Guenther, P. R. Schreiner, *Eur. J. Org. Chem.* **2012**, 5919–5927; c) G. Jakab, C. Tancon, Z. Zhang, K. M. Lippert, P. R. Schreiner, *Org. Lett.* **2012**, *14*, 1724–1727; d) Y. Takemoto, *Org. Biomol. Chem.* **2005**, *3*, 4299–4306; e) Z. Zhang, P. R. Schreiner, *Chem. Soc. Rev.* **2009**, *38*, 1187–1198.
- [11] Synthesis: a) A. Rostami, A. Colin, X. Y. Li, M. G. Chudzinski, A. J. Lough, M. S. Taylor, *J. Org. Chem.* **2010**, *75*, 3983–3992; b) Recent Application: L. Hu, M. Rombola, V. H. Rawal, *Org. Lett.* **2018**, *20*, 5384–5388.

- [12] V. Amendola, L. Fabbrizzi, L. Mosca, F.-P. Schmidtchen, *Chem. Eur. J.* **2011**, *17*, 5972–5981.
- [13] As cited in: A. J. Bard, L. R. Faulkner, *Electrochemical Methods: Fundamentals and Applications*, 2nd ed., Wiley, New York, **2001**, p. 339.
- [14] J.-M. Saveant, *J. Phys. Chem. B* **2001**, *105*, 8995–9001.
- [15] P. Pracht, F. Bohle, S. Grimme, *Phys. Chem. Chem. Phys.* **2020**, *22*, 7169–7192.
- [16] S. Grimme, *J. Chem. Theory Comput.* **2019**, *15*, 2847–2862.
- [17] S. Grimme, C. Bannwarth, S. Dohm, A. Hansen, J. Pisarek, P. Pracht, J. Seibert, F. Neese, *Angew. Chem. Int. Ed.* **2017**, *56*, 14763–14769; *Angew. Chem.* **2017**, *129*, 14958–14964.
- [18] For ORCA see: a) F. Neese, *Wiley Interdiscip. Rev.: Comput. Mol. Sci.* **2012**, *2*, 73–78; b) F. Neese, *Wiley Interdiscip. Rev.: Comput. Mol. Sci.* **2018**, *8*, e1327; c) for TURBOMOLE see: R. Ahlrichs, M. Baer, M. Haeser, H. Horn, C. Koelmel, *Chem. Phys. Lett.* **1989**, *162*, 165–169; d) O. Treutler, R. Ahlrichs, *J. Chem. Phys.* **1995**, *102*, 346–354.
- [19] C. Bannwarth, E. Caldeweyher, S. Ehlert, A. Hansen, P. Pracht, J. Seibert, S. Spicher, S. Grimme, *Wiley Interdiscip. Rev. Comput. Mol. Sci.* **2020**, <https://doi.org/10.1002/wcms.1493>.
- [20] J. G. Brandenburg, C. Bannwarth, A. Hansen, S. Grimme, *J. Chem. Phys.* **2018**, *148*, 064104.
- [21] S. Grimme, *Chem. Eur. J.* **2012**, *18*, 9955–9964.
- [22] C. C. Pye, T. Ziegler, E. van Lenthe, J. N. Louwen, *Can. J. Chem.* **2009**, *87*, 790.
- [23] a) Y. Zhao, D. G. Truhlar, *J. Phys. Chem. A* **2005**, *109*, 5656–5667; b) S. Grimme, J. Antony, S. Ehrlich, H. Krieg, *J. Chem. Phys.* **2010**, *132*, 154104; c) S. Grimme, S. Ehrlich, L. Goerigk, *J. Comput. Chem.* **2011**, *32*, 1456–1465; d) F. Weigend, R. Ahlrichs, *Phys. Chem. Chem. Phys.* **2005**, *7*, 3297–3305.
- [24] M. Rombola, C. S. Sumaria, T. D. Montgomery, V. H. Rawal, *J. Am. Chem. Soc.* **2017**, *139*, 5297–5300.
- [25] N. Busschaert, R. B. P. Elmes, D. D. Czech, X. Wu, I. L. Kirby, E. M. Peck, K. D. Henzdel, S. K. Shaw, B. Chan, B. D. Smith, K. A. Joffe, P. A. Gale, *Chem. Sci.* **2014**, *5*, 3617–3626.
- [26] a) G. Frey, J. N. Hausmann, J. Streuff, *Chem. Eur. J.* **2015**, *21*, 5693–5696; b) D. S. G. Henriques, K. Zimmer, S. Klare, A. Meyer, E. Rojo-Wiechel, M. Bauer, R. Sure, S. Grimme, O. Schiemann, R. A. Flowers II, A. Gansäuer, *Angew. Chem. Int. Ed.* **2016**, *55*, 7671–7675; *Angew. Chem.* **2016**, *128*, 7801–7805; c) N. Funken, F. Mühlhaus, A. Gansäuer, *Angew. Chem. Int. Ed.* **2016**, *55*, 12030–12034; *Angew. Chem.* **2016**, *128*, 12209–12213; d) W. Hao, X. Y. Wu, J. Z. Sun, J. N. C. Siu, S. N. MacMillan, S. Lin, *J. Am. Chem. Soc.* **2017**, *139*, 12141–12144; e) Y.-Q. Zhang, E. Vogelsang, Z.-W. Qu, S. Grimme, A. Gansäuer, *Angew. Chem. Int. Ed.* **2017**, *56*, 12654–12657; *Angew. Chem.* **2017**, *129*, 12828–12831; f) W. Hao, J. H. Harenberg, S. N. MacMillan, S. Lin, *J. Am. Chem. Soc.* **2018**, *140*, 3514–3517; g) C. Yao, T. Dahmen, A. Gansäuer, J. Norton, *Science* **2019**, *364*, 764–767; h) L. H. Leijendekker, J. Weweler, T. M. Leuther, D. Kratzert, J. Streuff, *Chem. Eur. J.* **2019**, *25*, 3382–3390; i) Z. Zhang, T. Hilche, D. Slak, N. Rietdijk, U. N. Oloyede, R. A. Flowers II, A. Gansäuer, *Angew. Chem. Int. Ed.* **2020**, *59*, 9355–9359; *Angew. Chem.* **2020**, *132*, 9441–9445.
- [27] a) M. Lankelma, A. M. Olivares, B. de Bruin, *Chem. Eur. J.* **2019**, *25*, 5658–5663; b) M. Zhou, M. Lankelma, J. I. van der Vlugt, B. de Bruin, *Angew. Chem. Int. Ed.* **2020**, *59*, 11073–11079; *Angew. Chem.* **2020**, *132*, 11166–11172; c) K. Lang, S. Torker, L. Wojtas, X. P. Zhang, *J. Am. Chem. Soc.* **2019**, *141*, 12388–12396; d) Y. Hu, K. Lang, C. Li, J. B. Gill, I. Kim, H. Lu, K. B. Fields, M. K. Marshall, Q. Cheng, X. Cui, L. Wojtas, X. P. Zhang, *J. Am. Chem. Soc.* **2019**, *141*, 18160–18169.

Manuscript received: October 9, 2020

Accepted manuscript online: October 21, 2020

Version of record online: January 12, 2021